

Symmetry breaking in a few-body system with magnetocapillary interactions

N. Vandewalle,¹ L. Clermont,¹ D. Terwagne,¹ S. Dorbolo,^{1,2} E. Mersch,¹ and G. Lumay^{1,2}

¹*GRASP, Physics Department, University of Liège, B-4000 Liège, Belgium*

²*F.R.S.-FRNS, B-1000 Bruxelles, Belgium*

(Received 25 April 2011; revised manuscript received 27 November 2011; published 13 April 2012)

We have experimentally investigated the interactions between floating magnetic spheres which are submitted to a vertical magnetic field, ensuring a tunable repulsion, while capillary forces induce attraction. We emphasize the complex arrangements of floating bodies. The equilibrium distance between particles exhibits hysteresis when the applied magnetic field is modified. Irreversible processes are evidenced. Symmetry breaking is also found for three identical floating bodies when the strength of the magnetic repulsion is tuned. We propose a DeJarguin-Landau-Verwey-Overbeek (DLVO)-like potential, i.e., an interaction potential with a primary and a secondary minimum, capturing the main physical features of the magnetocapillary interaction, which is relevant for self-assembly.

DOI: [10.1103/PhysRevE.85.041402](https://doi.org/10.1103/PhysRevE.85.041402)

PACS number(s): 83.80.Hj, 45.70.-n, 68.03.Cd, 47.55.Kf

I. INTRODUCTION

Many particles trapped at fluid interfaces lead to various patterns from fractal-like [1] to foam-like clusters [2]. The attractive interaction between floating bodies originates from the deformations of the fluid interface around the particles. This is called the “Cheerios effect” [3], a reference to clumping of cereal in a breakfast bowl. Despite being a subject with simple experiments and tricks, the fundamental and technological implications of the Cheerios effect are far from frivolous. Indeed, extensive researches are currently being undertaken to investigate the possibility of using surface tension to induce the self-assembly of small-scale structures. Understanding both shape and dynamics of the aggregate may enable much simplified manufacture of micro-electromechanical systems (MEMS) [4,5].

Experimental studies evidenced complex mechanisms and nonobvious patterns even for a low number of floating bodies [6]. Recent works [7,8,10] have been done with asymmetric bodies as well as unequal bodies. Computing with floating tiles for creating specific patterns has been also investigated [9].

In order to prevent aggregation, magnetic floating entities could be considered as proposed by Golosovsky *et al.* [11,12]. Indeed, dipole-dipole interactions could induce repulsive interactions leading to equilibrium distances between particles when placed in a confined system. We consider hydrophobic magnetic floating entities (see Sec. II for details). An external magnetic field is used for tuning the repulsion between bodies. Figure 1(b) shows pictures of the various configurations obtained for an increasing number of submillimeter floating objects (from $N = 6$ to 60 spheres) in a strong and uniform magnetic field. Since our system considers athermal particles only, it seems to exhibit symmetrical features, as expected from isotropic interactions [11]. Indeed, particles tend to be located at the vertices of a triangular lattice. However, some defects are observed in such small 2D crystals; i.e., fivefold symmetry is observed in the center of the rafts. Nearest neighbor distances are also larger at the cluster boundaries than in the center of the structure. Since no confinement potential is used in our experiments, those particular features can be interpreted as a result of the local curvature of the interface due to the size of the raft. A full description of such a curvature effect for

several hydrophobic objects can be found in [13]. This local curvature is also the origin of the nonequal interdistances that one observes on the pictures of Fig. 1(b).

Although it is possible to create crystals of noncontacting spheres for high magnetic field values, a decrease of the repulsive interaction always involves the appearance of disorder when beads come into contact. Figure 1(c) presents a crystal of $N = 28$ spheres which collapses when the magnetic repulsion is switched off. Particles always aggregate in disordered configurations, even after various “on-off” cycles. It should be noted that some pairs of particles remain in contact after switching again the field on.

The observations made in Fig. 1 raise fundamental questions. Why are local dense configurations not observed for a vanishing repulsion? How do particles get separated from each other? What is the origin of irreversibility? In the present paper, the case of simple configurations made of a low number of floating objects is investigated and fundamental characteristics of the magnetocapillary interactions are revealed. Those physical features will then be put into perspective for larger assemblies at the end of the paper.

II. EXPERIMENTAL SETUP

The experimental setup is the following. A large Petri dish is filled with water. The liquid-air interface is placed at the center of Helmholtz coils, as illustrated in Fig. 1(a). When a current i is injected in such coils, a uniform and vertical magnetic field \vec{B} is obtained in the Petri dish. Magnetic fields up to 50 G have been measured for current intensities up to $i = 2.5$ A. Chrome steel spheres (alloy AISI 52100, $\rho_s = 7830$ kg/m³) have been considered. Prior to experiments, spheres are washed with acetone and thereafter dried in an oven. As shown in [14], a chrome steel particle does not exhibit any hysteretic behavior and therefore its magnetization is completely reversible. As a result, one particle does not retain any residual magnetic moment once the field is removed. The onset of magnetization occurs immediately once $B > 0$ and is linearly dependent on B .

The diameter $D = 500$ μm of the spheres is lower than the capillary length $\lambda = \sqrt{\gamma/\rho_w g} \approx 2.5$ mm $\approx 5D$. Partial

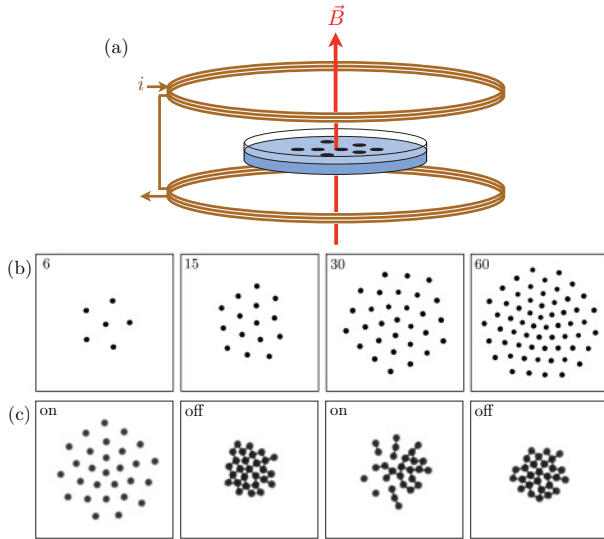


FIG. 1. (Color online) (a) Sketch of the experimental setup. A Petri dish filled with a liquid is placed at the center of horizontal Helmholtz coils. When a current i is injected in the coils, a vertical and uniform magnetic field B is produced through the air-liquid interface. There, floating objects were placed on the liquid surface before switching the field on. (b) Pictures of typical configurations obtained with an increasing number N of floating magnetic objects for a strong magnetic field ($Bo = 2.05$; see text). Large structures exhibiting a 5-fold symmetry are often encountered. (c) Four pictures of $N = 28$ floating bodies experiencing two “on-off” cycles. Starting from an ordered structure under a magnetic field (left picture), the system collapses when the field is switched off. Thereafter, the field is again increased and again switched off: The initial ordered structure is not recovered.

wetting ensures the floatability of the spheres. Indeed, they can float only in a hydrophobic case; the contact angle is therefore $\theta > 90^\circ$ (see Fig. 2). In most experiments, spheres are always separated from each other before relaxing the system. A high-resolution CCD camera records images from top. Image analysis allows the extraction of accurate interdistances r_{jk} for all pairs of floating bodies j and k . On recorded pictures, each particle has at least a diameter of 50 pixels, meaning that the accuracy for interdistances r_{jk} is less than $D/25$. On all plots (see Figs. 3 and 6), error bars are not drawn since they are smaller than the symbols.

As illustrated in Fig. 2 (top), the interaction between two magnetized spheres consists of (i) an attractive and horizontal capillary force F_γ due to the deformation of the air-liquid interface near floating objects, and (ii) a repulsive dipole-dipole magnetic force

$$F_m = \frac{3\mu_0\mathcal{M}^2}{4\pi r^4} \quad (1)$$

when the beads are far from each other [15]. The magnetization \mathcal{M} of the bodies is due to the vertical field B being proportional to the current i injected in the coils. Therefore, one has $F_m \sim i^2/r^4$.

Before conducting experiments, the magnetic repulsion F_m between beads was characterized since it represents the control parameter of our study. As illustrated in Fig. 2, two beads are placed in a watch glass with a curvature radius

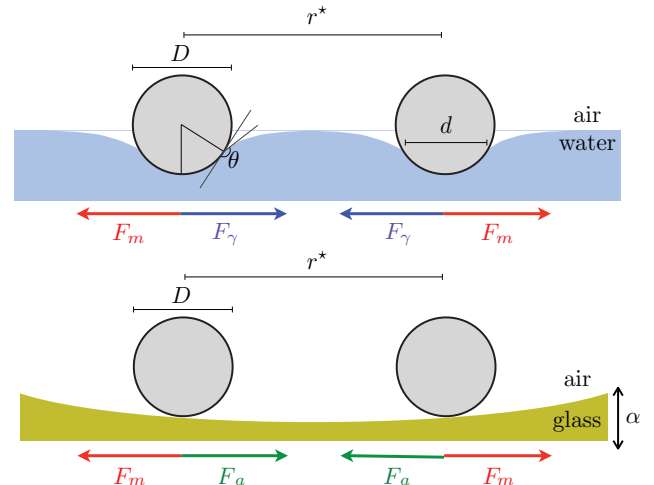


FIG. 2. (Color online) Illustration of forces acting on the beads in our experiments. Top: Interaction between two floating bodies at the air-liquid interface. Due to wetting of the bodies, deformations of the air-liquid interface implies the existence of a horizontal attractive force F_γ . The magnetization of each sphere induces a repulsive magnetic force F_m . The bodies are found at some equilibrium interdistance r^* where $F_\gamma = -F_m$. Bottom: On a curved surface which is slightly vibrated (reduced acceleration $\alpha \approx 1$), it is possible to determine the magnetic Bond number Bo_m characterizing the magnetic repulsion between beads by measuring the competition between F_m and the attractive force F_a due to surface curvature (see text).

$R = 0.1$ m. Then, the vertical magnetic field B is switched on to induce the dipole-dipole repulsive force F_m between the grains. The gravity force $F_a = -mgr/2R$, induced by the concavity of the watch glass, tends to gather the beads at the center of the watch glass. In order to avoid some sticking of the grains due to microscopic irregularities of the surface, the

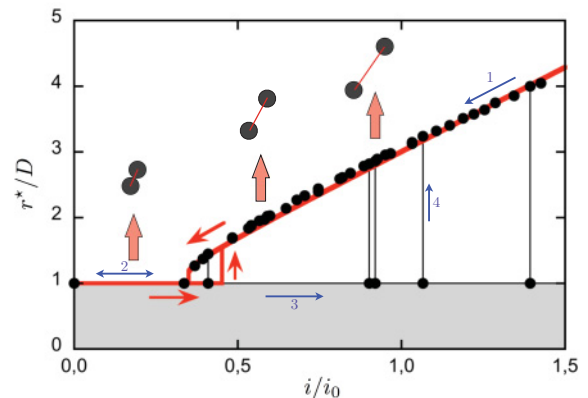


FIG. 3. (Color online) Dimensionless equilibrium interdistance r^*/D between two floating magnetized spheres as a function of the control parameter $\sqrt{Bo_m} = i/i_0$. Each dot represents an experiment. The gray region is forbidden since it corresponds to overlapping spheres. Thick curves correspond to a fit of the data with a model proposed in the text. Arrows indicate the way the system behaves around the hysteresis loop in the model [Eq. (7)]. Vertical lines corresponds to separation events of beads in repeated experiments, providing a broad distribution of bead detachment events. Numbered arrows are discussed in the text.

watch glass is vibrated vertically with a normalized maximum acceleration $\alpha = A\omega^2/g$ slightly higher than the unity. The vibration is switched off when the grains have reached a distance r^* of equilibrium and the repulsive force is calculated from $F_m = -F_a$. This measurement has been repeated five times for different values of the current i inside the coils and for large interdistances ($r^* > 3D$). Therefore, we obtained a relationship between the current i and the force ratio F_m/mg . This allows us to define the magnetic Bond number

$$\text{Bo}_m = \left(\frac{r^*}{2R}\right) \left(\frac{r^*}{D}\right)^4 \quad (2)$$

which will be used in scaling laws [see Eqs. (6) and (8)]. The second factor in $(r^*/D)^4$ takes into account the interaction range of F_m as seen in Eq. (1). In our experimental setup, $\text{Bo}_m = 1$ when the injected current $i_0 = 1.12$ A such that the control parameter becomes $\sqrt{\text{Bo}_m} = i/i_0$. In the following, we will use i/i_0 for simplicity.

III. RESULTS FOR $N = 2$

Let us now present the case of a pair of interacting floating spheres. Figure 3 presents the equilibrium distance r^*/D between two particles as a function of the control parameter i/i_0 . Each measurement is performed after waiting a minimum of 10 seconds for considering the quasistatic regime. This delay is indeed much larger than the characteristic time $\tau = \rho_s D^2/18\eta \approx 0.1$ s for velocity damping if one considers the Stokes force (by solving $m \frac{dv}{dt} = -3\pi\eta Dv$). As expected when attractive and repulsive forces compete, r^* depends on the magnetic interaction. For high field values, any modification of r^* through any variation of i/i_0 is reversible (see arrow 1). When the repulsion decreases below a threshold $i_{c1}/i_0 \approx 0.35$, the distance abruptly falls to contact. This transition is observed to be discontinuous, like in a first-order phase transition. Once a particle reaches this deformation, attraction starts to dominate the physical processes. Below this threshold, the particles remain “glued” by capillary forces (arrow 2). This “kiss” between two floating bodies is irreversible with respect to moderate magnetic field variations (arrow 3). In order to separate contacting bodies, a high magnetic field value (i_{c2}/i_0) is able to provide enough repulsion in some cases. The bead separation seems to be a probabilistic event (arrow 4) with a broad distribution of i_{c2}/i_0 values, as illustrated in Fig. 3. The contact-detachment events take place at different values of the control parameter, providing hysteresis in the system. In other cases, the maximum field produced in our experiment was not able to separate bodies. In that case, a mechanical separation was needed to reset the system. This clearly shows that two equilibrium positions exist.

The capillary interaction between two floating bodies is rather complex to describe [3]. This particular interaction is due to the overlap of interfacial deformations created by the particles. It should be noted that the superposition principle is not guaranteed such that the sum of deformations of neighboring floating objects does not correspond to the deformation of the whole assembly. One can understand that touching bodies create thin voids where the liquid tends to rise by capillary action. Complex deformation landscapes have also been evidenced experimentally and numerically using

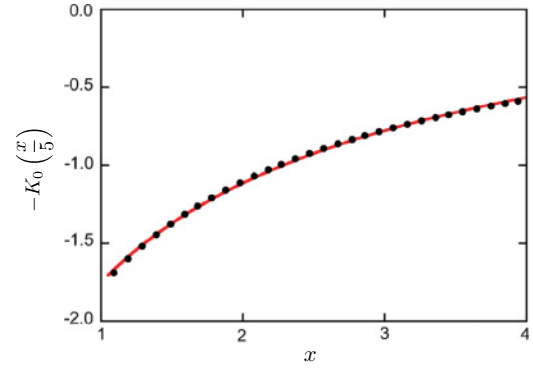


FIG. 4. (Color online) The continuous curves represent the attractive interaction potential U_γ [Eq. (3)] as a function of the dimensionless interdistance $x = r/D$ ranging between 1 (contact) and 4. The dots represent the approximated potential [Eq. (4)] as proposed in the main text. The agreement is excellent in the considered range of x values.

particles of various shapes and sizes [7]. The possible undulations of the contact line along the bodies creates capillary multipoles displaying various interaction types as described Kralchevsky *et al.* [16] and experimentally studied in [10]. All experimental and theoretical studies of the capillary attraction between two floating particles emphasize the complexity of the phenomenon and the occurrence of unexpected equilibrium states.

Using a few assumptions, Vella and Mahadevan [3] derived the interaction energy for two identical spherical particles. This interaction is given by

$$U_\gamma = -\Gamma K_0\left(\frac{r}{\lambda}\right) \quad (3)$$

where K_0 is the zero-order Bessel function of the first kind. The capillary energy Γ takes into account all physical ingredients such as the surface tension effects, sphere density, and the partial wetting of the bodies, including the contact angle θ . Since we typically consider interdistances between $r = D$ (contact) until $r \approx 4D$, the interaction potential may be approximated by

$$U_\gamma \approx -\frac{\tilde{\Gamma}\lambda D}{r-d} \quad (4)$$

which captures the main features of capillary attraction. The distance d corresponds roughly to the position of the meniscus on the bodies. Taking $d < D$ ensures the finiteness of the interaction energy when the bodies are in contact. Introducing the dimensionless parameter $x = r/D$, the validity of the approximation (4) is illustrated in Fig. 4 which presents $-K_0(x/5)$ (continuous curve), while dots corresponds to a fit with $A/(x-B) + C$ for x in the interval [1,4], $A = -3.72$, $B = -0.9$, and $C = 0.18$ being free fitting parameters. The approximation is acceptable and holds for all interdistances explored in our experiment. It should be noted that for larger values ($r > \lambda$), the approximation does not hold.

Considering the geometry of our system, the interaction energy between two point dipoles \mathcal{M} is $U_m = \mu_0 \mathcal{M}^2 / 4\pi r^3$, involving the expression of Eq. (1) for the magnetic force $F_m = -\frac{\partial U_m}{\partial r}$. When two magnetized spheres are placed close to contact, each spherical particle modifies the magnetization of

its neighbor and a deviation from Eq. (1) is therefore expected. Experimental evidence of this effect (close to bead contact) can be found in the work of Mehdizadeh *et al.* [17]. Although medium-range interactions are mainly considered in Ref. [18], strong deviations from the classical point dipole interaction are observed on the experimental data for $r < 2D$. In fact, the magnetization of each sphere comes from the external field plus the dipolar field generated by the neighboring sphere. We assume that the interaction energy can be approximated by

$$U_m \approx \frac{mgD^4\text{Bo}_m}{3(r-a)^3} \quad (5)$$

where a is a length characterizing the magnetization of the spherical beads, and Bo_m is the magnetic Bond number defined before [see Eq. (2)].

When both components of the interaction are put together, one has

$$U(r) \approx -\frac{\Gamma D}{(r-d)} + \frac{mgD^4\text{Bo}_m}{3(r-a)^3} \quad \text{for } r \geq D$$

$$= \infty \quad \text{for } r < D \quad (6)$$

which is illustrated in Fig. 5 as a function of the r/D for different strengths of the repulsive interaction, i.e., for different values of Bo_m . Like the DeJarguin-Landau-Verwey-Overbeek (DLVO) theory [19] for colloids, this potential $U(r)$ may exhibit a primary and a secondary minimum depending on the competition between capillary attraction and magnetic repulsion. The existence of two minima, often encountered at the microscopic scale, is a remarkable feature of our macroscopic system. When $\text{Bo}_m \ll 1$, only capillary forces are relevant and bodies comes to contact. The minimum of $U(r)$ is therefore $r_1^* = D$. When the repulsive force is high ($\text{Bo}_m > 1$), a second minimum r_2^* appears. The first derivative of $U(r)$ provides the location of this minimum

$$r_2^* = a + \frac{\xi D}{2} + \frac{1}{2}\sqrt{\xi D[\xi D - 4(d-a)]} \quad (7)$$

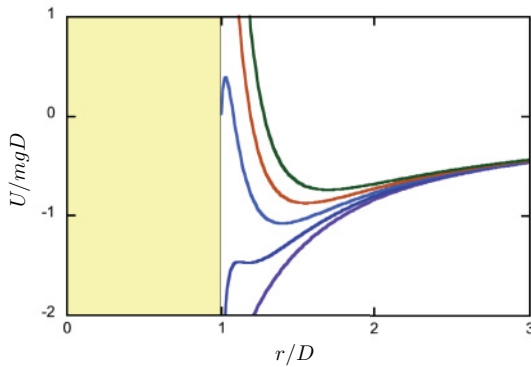


FIG. 5. (Color online) The dimensionless interaction potential U/mgD as a function of the dimensionless interdistance r/D for different strengths of the magnetic repulsion. The parameters of Eq. (6) are fixed by the fit of the data presented in Fig. 3. Depending on Bo_m , a primary and a secondary minimum can be observed. From top to bottom curves, one has $i/i_0 = 0.50, 0.45, 0.40, 0.35$, and 0.30 .

where the dimensionless number

$$\xi = \sqrt{\text{Bo}_m} \sqrt{\frac{mgD}{\Gamma}} \quad (8)$$

is the square root of the ratio of magnetic and capillary forces. Equation (7) has been fitted on the data of Fig. 3 and provides three parameter values $a = 0.7D$, $d = 0.92D$, and $\xi = 2.55 i/i_0$. The fitted values of a and d are below D as expected. The latter value informs us that capillary energy Γ is about 6.5 times larger than gravity energy mgD in our system, ensuring floatability of the beads. The model is in excellent agreement with the data, as seen in Fig. 3 (see thick curve). Moreover, it exhibits hysteresis. Indeed, the threshold i_{c1}/i_0 can be derived from the condition $\xi D = 4(d-a)$ in the last term of Eq. (7). This condition gives $i_{c1}/i_0 = 0.35$. When the repulsive force becomes much larger, the first minimum r_1^* disappears. This occurs at $i_{c2}/i_0 = 0.45$ using the parameters of the fit. The hysteretic behavior expresses the coexistence of two minima in between i_{c1}/i_0 and i_{c2}/i_0 . However, we have found experimentally numerous different values for the second threshold. This means that the detachment is sensitive to each particular contact. Indeed, the contact may change the partial wetting conditions which depends on the surface roughness of both spheres, as discovered in [6]. We did not observe any capillary rise in between the beads. However, the contact line anisotropy along each bead is a relevant effect and probably adds an extra force to be overcome for particle detachment. Since tiny deformations of the contact line are not reproducible, this explains also the various values of the current measured for detachment. The value $i_{c2}/i_0 = 0.45$ should then be considered as a low bound value, as observed in our experiments.

IV. RESULTS FOR $N = 3$

The case with 3 particles is now considered. In order to collect the data, we first tested the particles by pairs and we checked that each pair behaves like in Fig. 3. Figure 6 exhibits the distances for each pair in the $N = 3$ structure as a function of i/i_0 . Typical configurations are also shown. The data are shown for respectively a decrease and an increase of the current i/i_0 , i.e., for a complete cycle of bead magnetization. Memory effect is clearly observed. Moreover, symmetry breaking is seen since the different curves have different shapes and exhibit jumps at different i/i_0 values suggesting that the regularity of the structure is not conserved when capillary effects dominate the magnetic repulsion. This asymmetry takes place as follows.

When three particles are placed onto the liquid surface at high fields, a triangular configuration is obtained with identical interdistances (arrow 1). When the strength of the magnetic interaction decreases, the symmetry is suddenly broken: Two particles gather while the third one remains at some distance (arrow 2). When the capillary interaction becomes more and more important, a contact is seen between two particles while the distance to the third one vanishes (arrow 3). Finally, the spheres form a small cluster without a 3-fold symmetry. Two particles are still separated by a small distance. After contact, the magnetic field is kept to zero a moment before it increases again. Contrary to the case of two particles which could remain in contact even at large i/i_0 values, three spheres

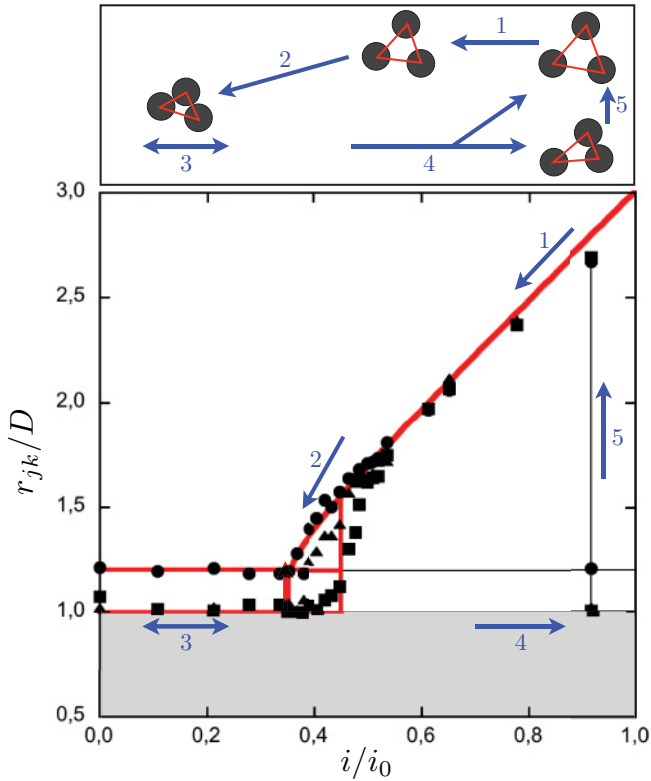


FIG. 6. (Color online) Dimensionless equilibrium distances r_{jk}^*/D for $N = 3$ floating spheres, as a function of the control parameter i/i_0 for a typical experiment. Each symbol represents a pair. The gray region corresponds to overlapping spheres. Thick curves represent the behavior obtained numerically when the model [Eq. (6)] is implemented for 3 particles. Numbered arrows indicate relevant steps discussed in the main text. Typical configurations are shown. Near arrow 1, repulsion dominates capillary attraction. One observes three beads located at the vertices of a regular triangle. Near arrow 3, three beads come into contact. As illustrated, a nonsymmetrical configuration is obtained in most cases, and this remains unchanged for a vanishing magnetic field. Near arrow 5, two different scenarios exist: either complete detachment restoring the system into a regular configuration or a partial detachment into a capillary dipole plus a single bead. The detachment takes place at high i/i_0 values.

separate without any perturbation above some probabilistic threshold (arrows 4 and 5). However, the way they separate is quite different from the way they come close together. Two scenarios exist: (i) In some cases, high field values restore a regular configuration, and (ii) in other cases one sphere separates from a pair of beads which remain in contact. When the experiment is repeated many times, the same scheme is observed but final configurations could present slightly different angles.

In order to model the behavior of three particles, we implemented numerically the potential of the trimer $U = U(r_{12}) + U(r_{23}) + U(r_{13})$ considering the relative positions of the particles along a 2D plane and Eq. (6). The parameters of the model are fixed with the values obtained for the $N = 2$ case, starting from a symmetrical equilibrium configuration, i.e., a regular triangle, for a large Bond number. The Bond number is then decreased step by step to zero. At each step,

the algorithm is searching for a minimum of the total energy U when beads are moving slightly around their previous location. A steepest descent deterministic method would keep the system into a regular triangle until the beads are touching at i_{c1}/i_0 . However, our algorithm considers the possible fluctuations for the sphere positions corresponding to at most $\sigma = D/20$ from their previous equilibrium positions (close to the accuracy of our measurements). These fluctuations could possibly originate from complex hydrodynamics interactions due to bead motions, contact line hysteresis, air turbulence, or simply the relaxation mechanism occurring after each modification of the magnetization. When i/i_0 decreases, the regular triangle shrinks, and around i_{c1}/i_0 , the beads come into contact in a nonsymmetrical configuration. Hard core potential is considered. Since the capillary attraction dominates, only small relative motions of contacting beads are observed for low i/i_0 values. Our model provides an interpretation of the phenomenon. In fact, the fluctuations for the bead motion allows the system to visit other local minima corresponding to asymmetric configurations. Indeed, local minima are provided by the coexistence of a primary and a secondary minimum observed in $U(r)$ (see Fig. 5). Please note that when i is close to i_{c1} , the energy barrier between both equilibrium situations is small. Fluctuations allows the system to jump from the regular configuration to the nonsymmetrical one.

The thick curves or lines on Fig. 6 represent the typical behavior obtained in numerical simulations. Since the parameters correspond to the $N = 2$ case, the curves are identical to the ones of Fig. 3. Contact and detachment take place respectively at $i/i_0 = i_{c1}/i_0 = 0.35$ and at $i/i_0 = i_{c2}/i_0 = 0.45$. The only difference with the $N = 2$ case is the presence of a second horizontal line between $i/i_0 = 0$ and i_{c2}/i_0 , corresponding to the symmetry breaking. This second line is a typical behavior obtained from our model.

We performed several simulations. The probability distribution function (PDF) of the relative distances r_{jk}/D obtained after 500 simulations is shown in Fig. 7 in a semilog plot.

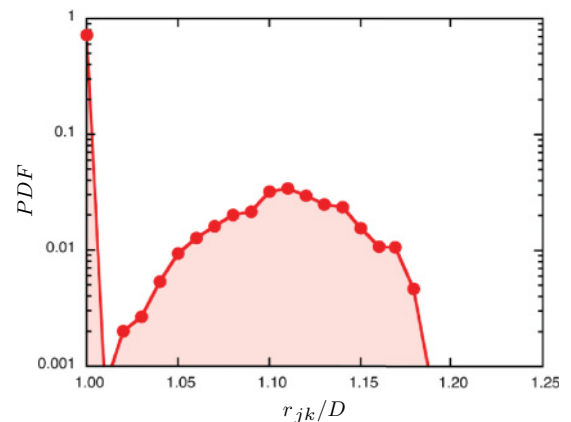


FIG. 7. (Color online) Probability distribution function (PDF) of interdistances r_{jk}/D obtained from 500 numerical simulations. Each simulation starts from a regular configuration at high magnetic field values. The repulsive interaction is then slowly decreased to zero. The interdistances are measured for final configurations. A peak appears at $r_{jk}/D = 1$ since beads are in contact. However, a broad distribution of r_{jk}/D values around 1.12 is observed meaning that the system lost its symmetry.

A peak at $r_{jk}/D = 1$ represents pairs of contacting beads expected for $i/i_0 < 0.35$. A broad Gaussian-like distribution of distances around $r_{jk}/D \approx 1.12$ is obtained revealing the probabilistic nature of the symmetry breaking process.

Recently, Berhanu and coworkers [2,6] have experimentally shown a similar behavior for 3 floating particles only submitted to capillary attraction. Due to friction between particles, nonsymmetrical configurations were obtained and quasilinear chains can be assembled [6]. Although bead-bead friction is not considered in the model, it could enhance the symmetry breaking and hysteresis observed in our experiments.

V. LARGER ASSEMBLIES ($N > 3$)

For larger assemblies ($N > 3$), the situation becomes more complex since a curvature centered on the assembly appears. This local curvature leads to capillary confinement of the central particles and smaller interdistances are therefore obtained near the center of mass. As a consequence, when Bo_m is reduced, dimers are first formed in the center of the structure which collapses. For a vanishing repulsion, a “loose” packing of spheres is obtained since trimers adopt nonsymmetrical shapes, as shown in the previous section. When the magnetic field is switched on, the ordered system is not restored due to hysteresis and capillary adhesion of dimers. One observes clearly on Fig. 2(c) that grains are still connected in that case even for high magnetic repulsion strengths. It is therefore hard to obtain close packed grains for a vanishing field. Further research should be done in

order to overcome those difficulties in order to control large magnetically self-assembled structures.

VI. CONCLUSION

In summary, we emphasized the main features of magneto-capillary interactions for a few-body system. The interaction potential exhibits one or two coexisting minima, providing memory effects, when repulsion is tuned. A DLVO-like model has been proposed to capture these features. It could be used for elaborating ways to shape self-assembled systems [20]. Experimentally, we discovered that a pair of floating bodies could remain in contact even for high repulsion values. Detachment is a probabilistic event which is related to various physical parameters such as wetting, friction, and capillary rise. Finally, the capillary interaction is found to limit the formation of dense arrangements.

By playing with magnetic field orientation and variations, one could change the nature of the interactions between beads. This could lead to a wide variety of arrangements [21]. The dynamical aspects of this experiment could also raise new fundamental questions, but this is left for future works.

ACKNOWLEDGMENTS

S.D. and G.L. thank FNRS for financial support. This work is financially supported by ESA through MAP Contract No. AO-99-108, the INANOMAT project (Grant No. IAP P6/17) of the Belgian Science Policy, and the University of Liege (Grant No. FSRC-11/36).

-
- [1] P. Meakin and A. T. Skjeltorp, *Adv. Phys.* **42**, 1 (1993).
 - [2] M. Berhanu and A. Kudrolli, *Phys. Rev. Lett.* **105**, 098002 (2010).
 - [3] D. Vella and L. Mahadevan, *Am. J. Phys.* **73**, 817 (2005).
 - [4] G. M. Whitesides and B. Grzybowski, *Science* **295**, 2418 (2002).
 - [5] J. A. Pelesko, *Self-Assembly* (Chapman & Hall, Boca Raton, 2007).
 - [6] M. J. Dalbe, D. Cosic, M. Berhanu, and A. Kudrolli, *Phys. Rev. E* **83**, 051403 (2011).
 - [7] J. C. Loudet and B. Pouligny, *Europhys. Lett.* **85**, 28003 (2009).
 - [8] J. C. Loudet and B. Pouligny, *Eur. Phys. J. E* **34**, 76 (2011).
 - [9] P. W. Rothmund, *Proc. Natl. Acad. Sci. USA* **97**, 984 (2000).
 - [10] A. B. D. Brown, C. G. Smith, and A. R. Rennie, *Phys. Rev. E* **62**, 951 (2000).
 - [11] M. Golosovsky, Y. Saado, and D. Davidov, *Appl. Phys. Lett.* **75**, 4168 (1999).
 - [12] M. Golosovsky, Y. Saado, and D. Davidov, *Phys. Rev. E* **65**, 061405 (2002).
 - [13] D. Vella, P. D. Metcalfe, and R. J. Whittaker, *J. Fluid. Mech.* **549**, 215 (2006).
 - [14] B. M. Shah, J. J. Nudell, K. R. Kao, L. M. Keer, Q. J. Wang, and K. Zhou, *J. Sound Vib.* **330**, 182 (2011).
 - [15] J. D. Jackson, *Classical Electrodynamics*, 3rd ed. (Wiley, New York, 1998).
 - [16] K. D. Danov, P. A. Kralchevsky, B. N. Naydenov, and G. Brenn, *J. Colloid Interface Sci.* **287**, 121 (2005).
 - [17] A. Mehdizadeh, R. Mei, J. F. Klausner, and N. Rahmatian, *Acta Mech. Sin.* **26**, 921 (2010).
 - [18] K. H. Taylor, Ph.D. thesis, University of Nottingham, 2009.
 - [19] J. N. Israelacvili, *Intermolecular and Surface Forces* (Academic Press, London, 2007).
 - [20] E. Edlund, O. Lindgren, and M. N. Jacobi, *Phys. Rev. Lett.* **107**, 085501 (2011); **107**, 085503 (2011).
 - [21] N. Vandewalle and M. Ausloos, *Phys. Rev. E* **51**, 597 (1995).